



Deformation and fatigue behaviors of carburized automotive gear steel and predictions

Bonglae Jo, Yongbo Shim

Iron and Steel Development Team, R & D Division of Hyundai Motor Company, 150, HyundaiYeonguso-ro, Namyang-eup, Hwaseong-si, Gyeonggi-do, Korea.

bl_jo@hyundai.com, simyongb@hyundai.com

Shahriar Sharifimehr, Ali Fatemi

Mechanical, Industrial and Manufacturing Engineering Department, The University of Toledo, 2801 W. Bancroft Street, Toledo, OH 43606, USA

Shahriar.sharifimehr@rockets.utoledo.edu, afatemi@eng.utoledo.edu

ABSTRACT. The fatigue behavior of carburized components such as automotive transmission gears is very complex due to hardness and microstructure difference, residual stresses and multi-axial stress states developed between the case and the core. In addition, automotive gears in service, commonly used in helical type, are actually subjected to complex stress conditions such as bending, torsion, and contact stress states. This study presents experimental and analytical results on deformation behavior of carburized steels, widely used in automotive gears, under cyclic stress conditions including axial and torsion loadings. Axial fatigue tests and rotating bending fatigue tests are also included. Predictions of cyclic deformation and fatigue behaviors of the carburized steel with two-layer model are compared with experimental results. The carburized steel investigated in this study exhibited cyclic softening under both axial loading and torsional loading. Predicted results with simple two-layer model for the cyclic deformation and fatigue behaviors were comparatively similar to the experimental data.

KEYWORDS. Carburizing; Case hardening; Gear steel; Cyclic softening; Fatigue; Prediction.

INTRODUCTION

Carburizing, one of the case hardening heat treatments, has been widely used in automotive parts due to significant improvements in component durability at a comparatively economic cost. The objective of carburizing of steels is to obtain a high-carbon plate type martensitic case with excellent wear, and good fatigue and pitting resistance in combination with a tough low-carbon core. In addition, the compressive residual stresses developed in the surface region result in a significant enhancement of the long life fatigue resistance of carburized steels.

Carburized steels consist usually of three regions with different microstructures, different hardnesses, and different material properties such as surface, and transition zone and core. Moreover, residual stresses developed by case hardening heat treatment and Poisson's ratio mismatch between the hard elastic case and the soft core usually cause multi-axial stress

states even when loaded with uniaxial load. Therefore, these complexities make it hard to understand exactly the deformation and fatigue behavior of carburized steels.

Generally gears in automotive transmission, a typical representative of carburized components, are subjected to complex stress conditions such as bending, torsion, and contact stress states due to continuous engagement with their mating gears. Therefore, when designing an actual transmission gear it is very important to understand the deformation and fatigue behavior under the combined stress conditions and to predict its fatigue life. However, there has been a little research on the deformation and fatigue behavior of carburized steels with case-core sections under complex stress conditions, although they have been used in automotive transmission for many years.

There have been several investigations on the deformation and fatigue behavior of carburized steels including prediction analysis. Yin and Fatemi [1] studied monotonic and cyclic deformations of carburized SAE 8620 steels including residual stress effects. Both the carburized (i.e. case-core material) and the core materials exhibited cyclic softening, while the case material exhibited cyclic hardening. The carburized cyclic stress-strain curve was close to that of the core material in the plastic deformation region. They also predicted monotonic and cyclic axial deformation behavior using both two-layer and four-layer models, resulting in predicted monotonic deformation curves of the carburized specimens being close to the experimental curve, but the predicted cyclic curve was higher than the experimental curve.

Baumel et al. [2] proposed multi-layer model for fatigue life calculations of nitrided (case-hardened) 50CrMo4 steel, where the critical cross section of case-hardened components is modeled by multiple layers. Within each of the layer, material properties, residual stresses and the strains caused by external loading are assumed to be constant. In the case of axial loading, the strain is determined by using the equilibrium condition that sum of the internal axial forces has to be balance the external load. In case of rotating bending, the stresses and the strains across the cross section are obtained by loading the component with two normal bending moments that have the same amplitude, with bending axis perpendicular to each other. They showed that predicted fatigue life and crack initiation locations were good agreement with the experimental data, for the strain-controlled axial fatigue tests and load-controlled rotating bending fatigue tests.

Bomas [3] applied the weakest link model to describe fatigue failure of carburized 16MnCr5 and 16MnCrS5 steels, based on the assumption that material strength is determined by the weakest site in the stressed region. Two main fatigue nucleation sites were considered: the surface due to roughness or surface oxidation, and the bulk. Unnotched case-hardened specimens with different geometries, different mean stresses and different carburizing processes were subjected to different loading conditions, including rotating bending, plane bending and push-pull loading. Their method was shown to be reasonable in predicting the fatigue limit of carburized steels. However, determining the method requires finding empirical parameters.

Zhang et al. [4] studied three-point bending fatigue behavior of induction-hardened shafts made of SAE 1045 steel. Considering that the shafts have multiple hardness layers with constant cyclic deformation and fatigue properties, prediction for crack nucleation life was made by using Morrow and Smith-Watson-Topper mean stress correction model. They showed that predicted life was good agreement with the experimental fatigue lives.

Yin and Fatemi [5] studied axial fatigue behavior and life prediction of carburized SAE 8620 steel specimens. The strain-life curve for the carburized specimen (case-core material) was close to that of the case material in the long life regime, while in the short life regime the curve was in between the curves for the case and the core materials. Sub-surface failure in the long life regime and surface failure in the short life region occurred, and, the shift from surface to sub-surface nucleation occurred at the intersection of the strain-life curves of the case and the core materials. They also used both a two-layer model and a four-layer model to predict fatigue life, resulting in a good match between the experimental and calculated results for the carburized specimens except for some points in the very short life region, when applying the upper-bound method. This method assumes that the longest life of the different layers is used as the fatigue life.

Shamsaei and Fatemi [6] studied torsional cyclic deformation and fatigue behavior of induction hardened (case-hardened) solid round specimens made of 1050 steel. They showed that under torsional loading induction hardened 1050 steel exhibited cyclic softening, and most of the torque is carried by the case due to the higher level of stress in the case. They also predicted cyclic shear deformation behavior for the case and the core materials by using the common criteria based on their respective axial behavior, resulting that von Mises criterion predicted well the shear deformation curves for the case and the core, while the Tresca and maximum principal strain criteria significantly under-estimated and over-estimated the shear stress amplitude, respectively.

In this study, for better understanding the cyclic deformation and fatigue behavior of carburized steel, monotonic and cyclic deformation tests under both axial and torsional loading conditions were performed. Axial and rotating bending fatigue tests were also conducted. In addition, predictions of cyclic deformation and fatigue behaviors of the carburized steels investigated using a two-layer model are presented and compared with experimental results.



MATERIAL AND EXPERIMENTAL PROCEDURES

The material used in this study was Cr-Mo steel, which is widely used for automotive gears. The chemical composition of this steel is shown in Tab. 1. Two types of round specimens were used in this study and their geometries are shown in Fig. 1. Type 1 specimens were used for axial monotonic and cyclic test, axial fatigue test and rotating bending fatigue tests. Type 2 specimens were used for monotonic and cyclic torsional tests.

All specimens were machined and ground after homogenization treatment of steel bars at 930°C. The specimens were then vacuum carburized at 860°C with acetylene gas, and quenched by using high pressured helium gas. Fig. 2 shows the microstructure of surface and core in a cross-section of the type 2 specimen. Typically, the surface was high carboned plate-type martensite and retained austenite, and the core was mixed tempered lath-type martensite and bainite.

Fig. 3 shows the hardness profiles of the specimens, along with the approximated hardness profile used in predictions. The surface and the core hardnesses were about Hv 760 and Hv 400 for type 1 specimens, and Hv 810 and Hv 320 for type 2 specimens, respectively. As shown in this figure, measured hardness profiles show that the transient region between the case and the core is thin. Therefore, a two-layer model with two different hardness values was considered for analysis and predictions in this study.

Monotonic and cyclic axial tests were conducted with type 1 specimens, according to ASTM standard. A closed-loop servo-hydraulic axial load frame in conjunction with a digital servo-controller and hydraulically operated grips were used for the tests. The multiple step test method was used to obtain cyclic material properties. A sinusoidal waveform was applied.

C	Si	Mn	P	S	Cr	Mo	Nb	Fe
0.18	0.10	0.68	0.011	0.015	1.29	0.60	added	bal.

Table 1: Chemical compositions (in weight %).

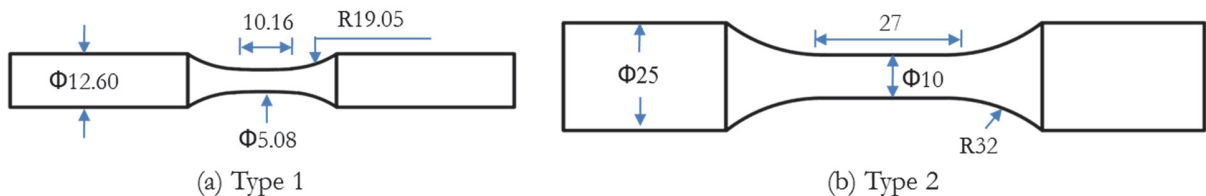


Figure 1: Specimen configuration and geometry (in mm).

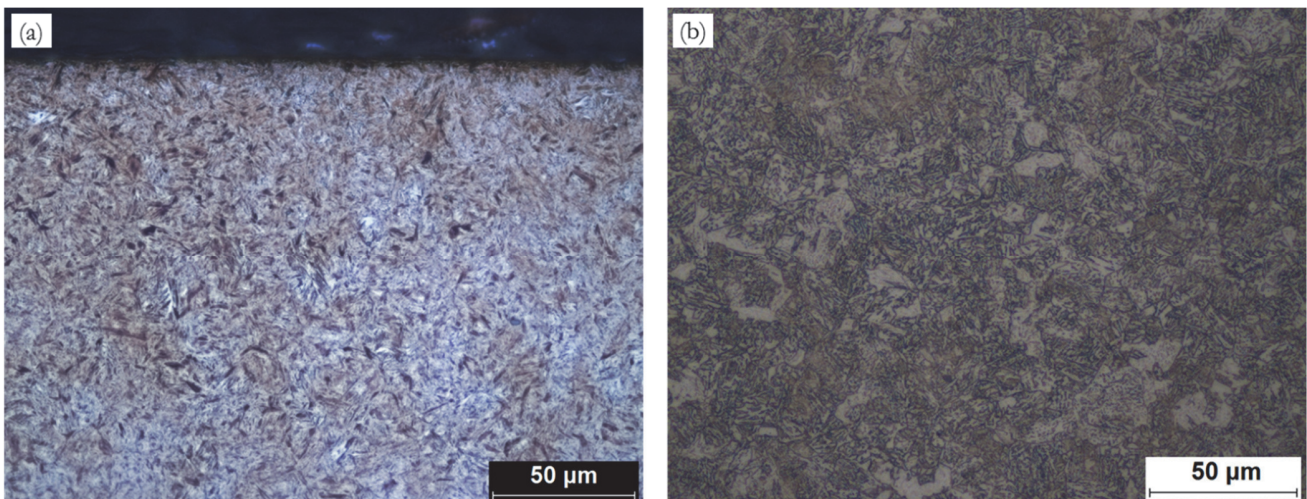


Figure 2: Microstructure of the carburized specimens in (a) the surface and, (b) the core.

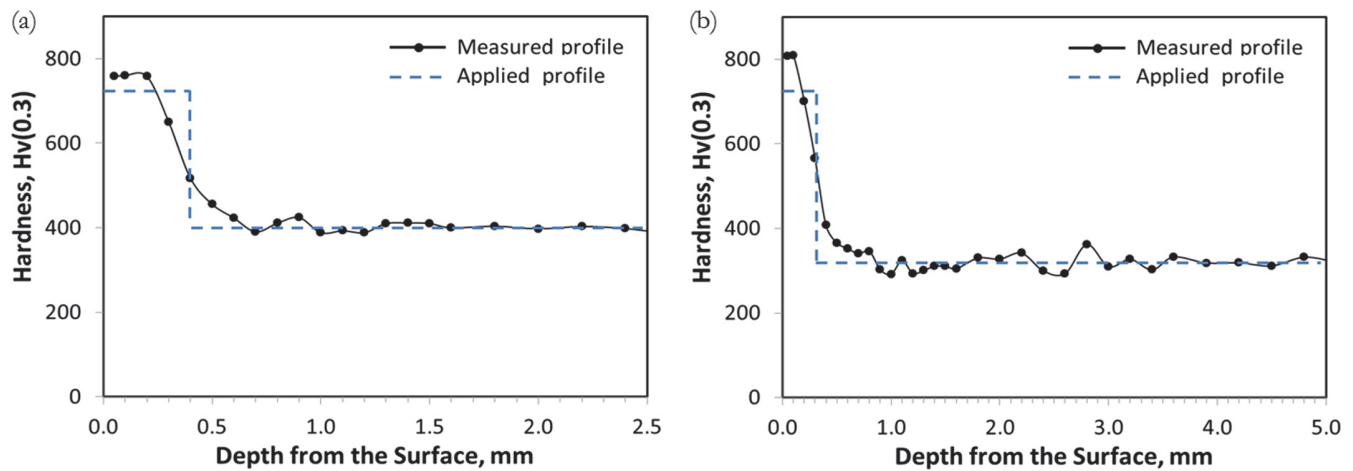


Figure 3: Measured hardness profile superimposed with approximated hardness profile of (a) type 1 specimen and, (b) type 2 specimen.

For each axial strain amplitude level, sufficient cycles were applied to get a stable hysteresis loop. Monotonic and cyclic torsion tests with type 2 specimens were also performed according to ASTM standard, and by using a closed-loop servo-hydraulic axial-torsional load frame in conjunction with a digital servo-controller and hydraulically operated grips.

In order to investigate the fatigue behavior of carburized specimens, axial fatigue tests and rotating bending fatigue tests with type 1 specimens were performed under load-controlled, fully reversed condition ($R=-1$). Rotating bending fatigue tests were conducted at a load frequency of 28.75 Hz, with a constant bending moment along the length of the specimens. For all failed specimens, fracture surfaces were observed to ensure the main failure mode of each test specimen, such as sub-surface or surface initiated failure.

EXPERIMENTAL RESULTS, PREDICTIONS AND DISCUSSION

Monotonic and Cyclic Axial Deformation Behaviors

The monotonic and cyclic axial deformation behavior of the materials can be expressed well by a Ramberg-Osgood type equation as:

$$\varepsilon = \varepsilon_e + \varepsilon_p = \frac{\sigma}{E} + \left(\frac{\sigma}{K}\right)^{1/n} \quad (1)$$

where ε , ε_e , ε_p , σ , E , K and n are total true strain, true elastic strain, true plastic strain, true stress, elastic modulus, strength coefficient, and strain hardening exponent, respectively. For cyclic loading, stress amplitude (σ_a or $\Delta\sigma/2$) and strain amplitudes (ε_a or $\Delta\varepsilon/2$) are used in Eq. (1) and K and n are replaced by cyclic strength coefficient, K' , and cyclic strain hardening coefficient, n' , respectively.

Monotonic and cyclic properties for the carburized (case hardened) specimens measured are shown in Tab. 2. The cyclic stress-strain curve is superimposed with the monotonic stress-strain curve in Fig. 4(a). Both the monotonic and cyclic deformation behaviors are well represented by the Ramberg-Osgood relation. Similar to previous results on the case-hardening steel [1], this carburized steel also exhibits cyclic softening behavior.

Since cyclic axial deformation data for neither the case nor the core were available for this material, predictions were performed by using the data of other case-hardening material [5, 7], on the basis of similar hardness level and similar microstructure. The values of K' and n' for both the case and the core are presented in Tab. 2.

A two-layer model divided into a hardened case and a softer core was used to predict the cyclic deformation behavior of the carburized specimens. As shown in Fig. 3, type 1 specimens consist of a 0.4 mm thick case with constant hardness of Hv 740 and a core layer with constant Hv 400. Type 2 specimens had a 0.3 mm thick case with constant hardness of Hv 740 and a core layer with constant Hv 320. The rule of mixture based on equilibrium condition was used to predict the stress for carburized specimens, given as:



$$\sigma = \sigma_{\text{case}} \frac{A_{\text{case}}}{A} + \sigma_{\text{core}} \frac{A_{\text{core}}}{A} \quad (2)$$

where σ is the average stress for the carburized specimen and A is the total cross section area. From approximated material properties of both the case and the core layer, the deformation behavior of the carburized specimen was predicted and compared with experimental results.

Predicted and experimental cyclic stress-strain curves are shown in Fig. 4(b). As can be seen from this figure, the predicted curve is a little bit underestimated, but comparatively similar to the experimental curve. This indicates that a simple two-layer model can be used to predict the cyclic deformation behavior for the carburized steel in the absence of real data. The small gap between the predicted and experimental data is attributed to the difference of microstructural and mechanical properties between the two core materials investigated. As an example, the beneficial influence of grain refinement on the mechanical properties such as strength and fatigue limit in steel could be well explained by Hall-Petch equation which indicates that the strength of a metal is proportional to the inverse of the square root of the grain size. And also, grain refinement (grain size reduction) is a method to increase the toughness of a metal. Therefore, it is estimated that the predicted curve will be even closer to the experimental data, considering that the material used in this study has a finer grain, as shown in Fig. 2, resulting in superior mechanical properties to those of the core material used for prediction.

	Monotonic					Cyclic		
	E (GPa)	S _y (MPa)	EL. (%)	K (MPa)	n	K' (MPa)	n'	S' _y (MPa)
Carburized	201	1025	2.82	3883.6	0.1637	2633.5	0.1294	-
Case	208	1125	1.7	11109	0.372	16053	0.289	2665
Core	214	990	27	2276	0.138	2137	0.134	927

Table 2: Axial monotonic and cyclic deformation properties of the material investigated.

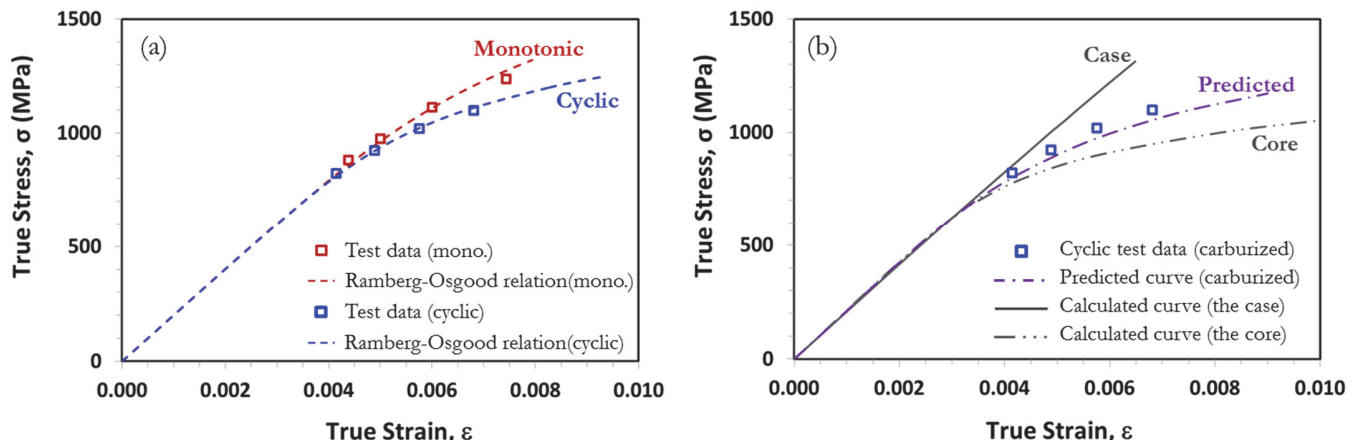


Figure 4: Monotonic and cyclic axial deformation behaviors (a) and prediction curves (b).

Monotonic and Cyclic Torsional Deformation Behaviors

The monotonic and cyclic torsional deformation behavior of the materials can be also expressed by a Ramberg-Osgood type equation as:

$$\gamma = \gamma_e + \gamma_p = \frac{\tau}{G} + \left(\frac{\tau}{K_o}\right)^{1/n_o} \quad (3)$$

where γ , γ_e , γ_p , τ , G , K_o and n_o are total shear strain, elastic shear strain, plastic shear strain, shear stress, shear modulus, shear strength coefficient, and shear strain hardening exponent, respectively. For cyclic loading, stress amplitude (τ_a or $\Delta\tau/2$) and strain amplitudes (γ_a or $\Delta\gamma/2$) are used in Eq. (3) and K_o and n_o are replaced by cyclic strength coefficient, K'_o , and cyclic strain hardening coefficient, n'_o , respectively.

Monotonic shear deformation behavior for the carburized (case hardened) specimens is well represented by the Ramberg-Osgood relation. The measured shear properties are shown in Tab. 3. Fig. 5(a) illustrates monotonic and cyclic torque-strain behavior, showing that this carburized steel exhibits also cyclic softening behavior under torsional loading, similar to cyclic softening obtained from a thick case obtained from induction hardened steel in [6]. And also, the cyclic fatigue crack was found to be nucleated on the surface and to be propagated along about 45° helix (spiral crack pattern), which is the plane of maximum principal strain.

	Monotonic shear				Axial cyclic		
	G (GPa)	τ_y (MPa)	K_o (MPa)	n_o	K' (MPa)	n'	S_y' (MPa)
Carburized	77.47	498.5	1703	0.1977	-	-	-
Case	80.00	-	-	-	16053	0.289	2665
Core	74.62	-	-	-	2041	0.193	613

Table 3: Monotonic shear deformation properties of the carburized steel and axial cyclic properties of the materials investigated

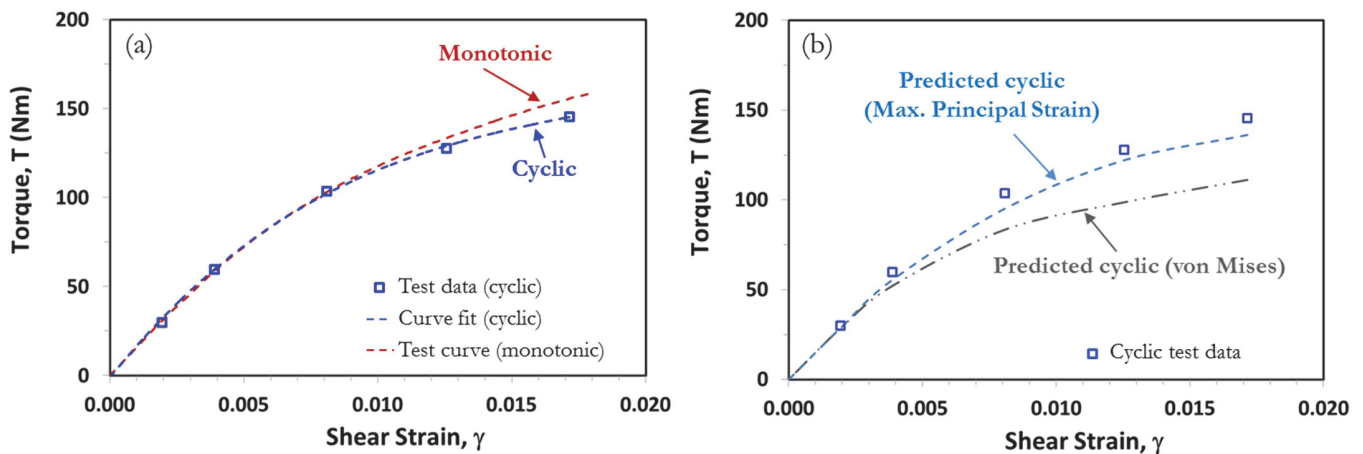


Figure 5: (a) Monotonic and cyclic torque-strain behavior and, (b) Predicted vs. experimental cyclic stress-strain curves

For predictions, since cyclic shear strength coefficient, K'_o , and cyclic shear strain hardening exponent, n'_o , data for neither the case nor the core were widely available, predictions were performed by using the axial cyclic data of another case-hardening material [5, 7] on the basis of similar hardness level and similar microstructure. The axial cyclic data used in this prediction are presented Tab. 3. In this case, the following criteria were used to relate shear properties to axial properties:

$$\text{von Mises: } K'_o = \frac{K'}{\sqrt{3}} \left(\frac{1}{\sqrt{3}} \right)^{n'} \quad \text{and} \quad n'_o = n' \quad (4)$$

$$\text{Maximum Principal Strain: } K'_o = \frac{K'}{1+\nu} \left(\frac{1}{2} \right)^{n'} \quad \text{and} \quad n'_o = n' \quad (5)$$

The value of Poisson ratio, ν , used in this study was 0.3.

The shear stress-strain relationships for both the case and the core sections were calculated by using above criteria, and then the total torque carried by the carburized specimens was obtained. At high strain region, yielding of the core material was also considered. The total torque of the carburized specimen can then be calculated from:

$$T_{total} = T_{core} + T_{case} = 2\pi \int_0^{a_{core}} \tau r^2 dr + 2\pi \int_{a_{core}}^{D/2} \tau r^2 dr \quad (6)$$

where a_{core} is the core radius, D is the diameter of the specimen, and τ is the shear stress at radius r .

Fig. 5(b) shows the predicted results. As shown in this figure, for this carburized steel, maximum principal strain criterion is in good agreement with the experimental data, whereas von Mises criterion significantly under-estimates the cyclic



stress-strain curve. This result is well consistent with the failure pattern observed (spiral crack pattern). However, this result is dissimilar to that of induction hardening steel showing that the shear deformation curves were predicted well by von Mises criterion [6]. This is attributed to the different depth of surface hardening layer and the different microstructures of the core between the carburized and induction hardened steel.

Axial and Rotating Bending Fatigue Behaviors

For fully reversed straining, total strain amplitude-fatigue life of small smooth axial specimens can be expressed by the following equation as:

$$\frac{\Delta\varepsilon}{2} = \varepsilon_a = \frac{\Delta\varepsilon_e}{2} + \frac{\Delta\varepsilon_p}{2} = \frac{\sigma'_f}{E} (2N_f)^b + \varepsilon'_f (2N_f)^c \quad (7)$$

where σ'_f , b, ε'_f , c and $2N_f$ are the fatigue strength coefficient, the fatigue strength exponent, the fatigue ductility coefficient, the fatigue ductility exponent and the number of reversals to failure, respectively. The stress amplitude-fatigue life behavior is represented by the first elastic term from Eq. (7), Basquin-type equation as:

$$\frac{\Delta\sigma}{2} = \sigma_a = \sigma'_f (2N_f)^b \quad (8)$$

The rotating bending fatigue behavior can be also expressed by Basquin-type equation.

Fig. 6 shows axial fatigue and the rotating bending fatigue test results of the carburized specimens, along with its respective Basquin-type fitted equations. For obtaining the σ'_f and b values, surface failure and run-out data were not included on this equation fit. The measured values of σ'_f and b were 2316 MPa and -0.059 for rotating bending fatigue and 2179 MPa and -0.077 for axial fatigue, respectively. Failure mode of both the axial and the rotating bending was mostly sub-surface cracking, except for high load amplitude region with surface cracking, which was likely attributed to relaxation of surface compressive residual stress on the surface.

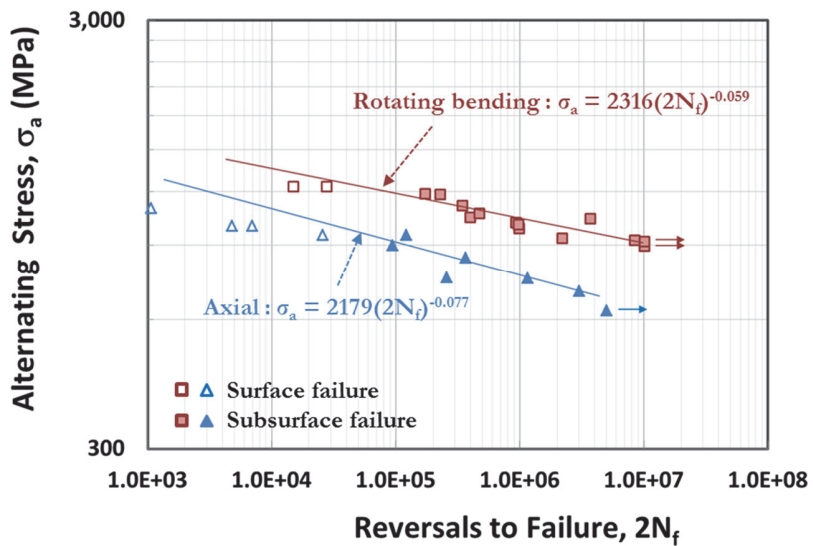


Figure 6: Composite plot of S-N curves for axial and rotating bending fatigue of the carburized specimens.

Fig. 7 represents fracture surface of both axial fatigue specimen and the rotating bending fatigue test specimen showing sub-surface failure at around 10^6 cycles. The depth of sub-surface crack nucleation sites for the rotating bending was about 0.6 mm below the surface, closer distance from the surface than that for the axial loading of about 1.0 mm. This seems to be due to stress gradient difference between rotating bending and axial loading.

Commonly, the fatigue limit for axial loading can range from 0.75 to 0.9 of the rotating bending fatigue limit for small smooth unnotched specimens [8]. For this carburized steel, as shown in Fig. 6, the fatigue strength of axial loading is about 70% of that of rotating bending specimen on the basis of fatigue strength at 10^6 cycles, slightly lower than that of

commonly expected. It seems that the stress gradient effect between axial loading and rotating bending is more significant for case hardening steel.

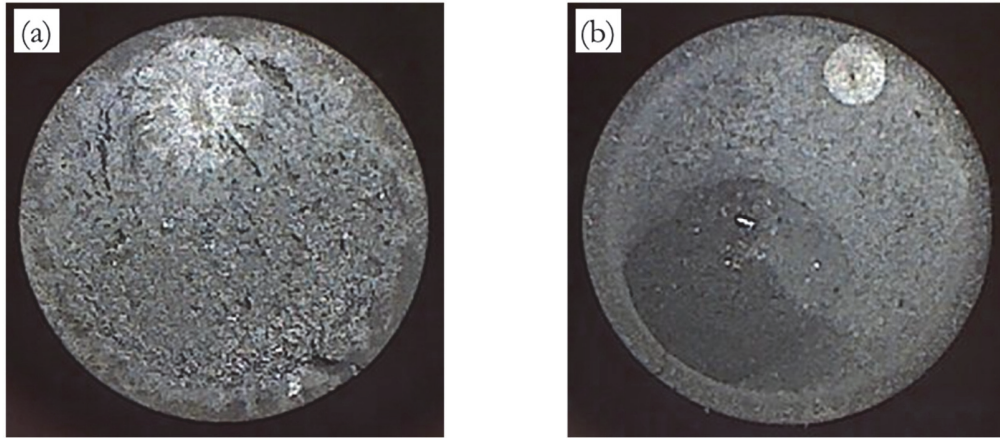


Figure 7: Photos of sub-surface failure of the carburized specimens at around 10^6 cycles under (a) axial loading (701 MPa, 1.5×10^6 cycles) and (b) rotating bending (1038 MPa, 1.83×10^6 cycles).

The two-layer model based on the total forces equilibrium condition was also used to predict the long life fatigue behavior of carburized specimens. Values of σ_f' and b for both the case and the core from [5, 7] were used to predict the both axial and rotating bending fatigue behaviors of the carburized steel. Axial force equilibrium for axial loading and bending moment equilibrium for rotating bending were assumed for predictions. In addition, the fatigue strength for axial loading was assumed to be 75% of the bending fatigue strength at a given life. The effect of residual stresses on predictions of fatigue life for sub-surface failures was not considered, because it is estimated that the magnitude of compressive or tensile residual stresses at the area near the fatigue crack nucleation, as shown in Fig. 7, would be small enough to ignore. Fig. 8 illustrates the experimental data and the predicted results for this carburized steel, and superimposed estimated S-N curves for both the case and the core materials. For both axial fatigue and rotating bending fatigue, the experimental data of the carburized specimens are mostly in between the estimated case and the core curves, more close to the case curve at long life region. The predicted results are comparatively similar to the experimental data, except for surface failure region at short life, which is in the high load amplitude regime. This indicates that this simple method may provide a useful guide for estimation of axial and rotating bending fatigue life at long-life region, in the absence of any fatigue data.

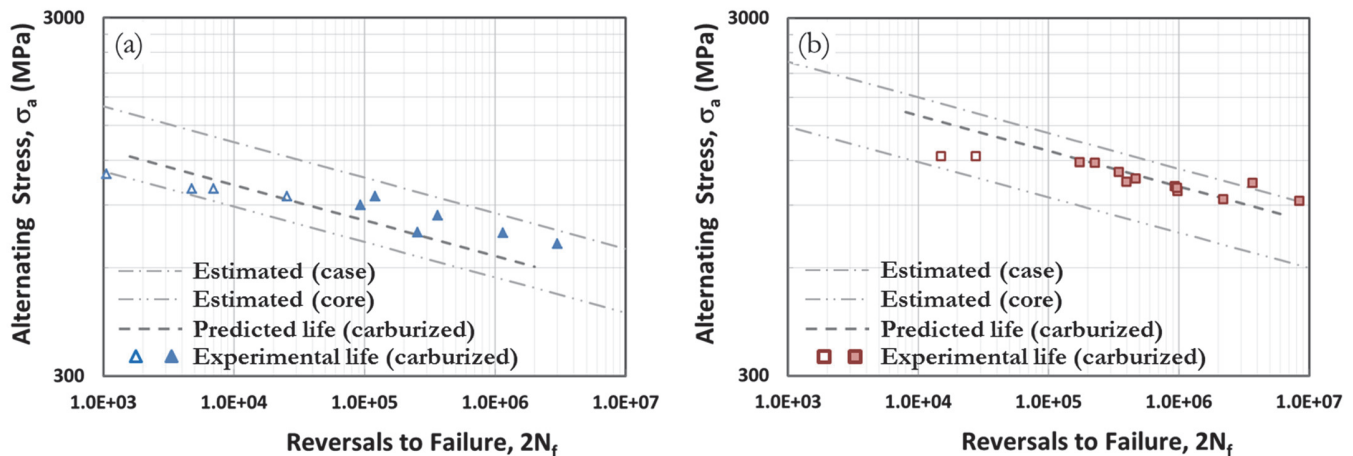


Figure 8: Fatigue test data and prediction results for (a) axial loading and (b) rotating bending.

The axial strain-life curve of the carburized specimen was compared with those of both the case and the core materials. The strain amplitude of the carburized steel used in this study was estimated from cyclic deformation curve measured with



same geometry specimen. The strain-life curves of both the case and the core material were estimated by using Roessle and Fatemi's equation [9] as:

$$\varepsilon_a = \frac{4.25(HB)+225}{E} (2N_f)^{-0.09} + \frac{0.32(HB)^2-487(HB)+191000}{E} (2N_f)^{-0.56} \quad (9)$$

Fig. 9 presents the axial strain-life data of the carburized specimen and estimated the axial strain-life curve of the case and the core material. It can be seen from this figure that in the long-life region (sub-surface cracked failure region), the experimental data of the carburized specimens are in between the case and the core curves, but more close to the case curve, similar to previous results on the case-hardening steel [5]. In the short-life region (surface cracked failure region) the carburized data are below both the case and the core curves.

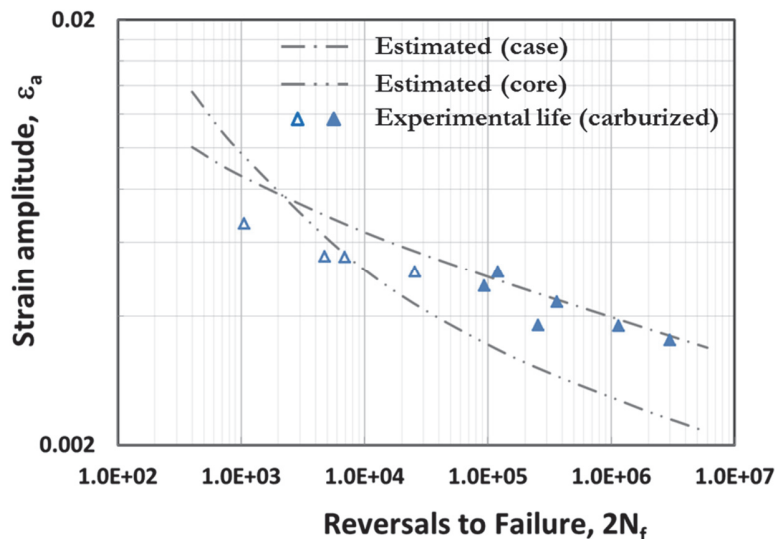


Figure 9: Superimposed strain-life curves for the case and the core and prediction results.

CONCLUSIONS

This study was carried out for better understanding the cyclic deformation and fatigue behavior of carburized steel. Monotonic and cyclic deformation tests under both axial and torsional loading conditions were performed. Axial and rotating bending fatigue tests were also conducted. Based on the experimental results and analysis presented here, the following conclusions can be made:

- 1) The carburized steel investigated in this study exhibited cyclic softening under axial loading. Predicted curve based on the two-layer model for the cyclic deformation behavior was a little under-estimated, but comparatively similar to the experimental curve.
- 2) Under torsional loading, the carburized steel exhibited cyclic softening behavior. Predicted results for cyclic shear deformation showed that the maximum principal strain criterion provides good agreement with the experimental data, whereas von Mises criterion significantly under-estimates the cyclic stress-strain curve.
- 3) Failure mode of both the axial and the rotational bending was mostly sub-surface cracking, except for high load amplitude region with surface cracking. For this carburized steel, the fatigue strength of axial loading was about 70% of that of rotating bending specimen on the basis of fatigue strength at 10⁶ cycles, slightly lower than that of commonly expected. This seems to be due to stress gradient effects being more significant for carburized steels.
- 4) For both axial fatigue and rotating bending fatigue, the predicted results based on the simple two-layer model were comparatively similar to the experimental data, except for surface failure region at short life.



REFERENCES

- [1] Yin, F., Fatemi, A., Monotonic and cyclic deformations of case-hardened steels including residual stress effects, *Strain-An Int. J. for Experimental Mechanics*, 47 (2011) E74-E83.
- [2] Baumel, A. J., Seeger, T., The influence of residual stresses and surface strengthening on components fatigue life. In: *Fatigue 90*, Vol. 1 (1990) (Edited by H. Kitagawa and T. Tanaka), Honolulu, HI, USA, 311-316.
- [3] Bomas, H., Mary, P., Schleicher, M., Calculation method for the fatigue limit of parts of case hardened steels, *Mater. Sci. Eng. A*, 234 (1997), 393-396.
- [4] Zhang, H. Y., Stephens, R. I., Glinka, G., Sub-surface fatigue crack initiation and propagation behavior of induction-hardened shafts under the effects of residual and applied bending stresses. In: *Fatigue and Fracture Mechanics*, vol. 30 (2000) (Edited by K. L. Jerina and P. C. Paris). ASTM STP 1360, ASTM, West Conshohochen, PA, USA, 240-260.
- [5] Yin, F., Fatemi, A., Fatigue behavior and life predictions of case-hardened steels, *Fatigue and Fract. Eng. Mater. Struct.*, 32 (2009) 197-213.
- [6] Shamsaei, N., Fatemi, A. Deformation and fatigue behaviours of case-hardened steels in torsion: experiments and predictions, *Int. J. of Fatigue*, 31 (2009) 1836-1839.
- [7] American Iron and Steel Institute (AISI), Bar Steel Fatigue Database, <http://barsteelfatigue.autosteel.org>
- [8] Stephens, R.I., Fatemi, A., Stephens, R.R., Fuchs, H.O., *Metal Fatigue in Engineering*, 2nd ed., Wiley Interscience, (2000).
- [9] Roessle, M. L., Fatemi, A. Strain-controlled fatigue properties of steels and some simple approximations, *Int. J. of Fatigue*, 22 (2000) 495-511.